

# Active Regulation of On-Demand Drug Delivery by Magnetically Triggerable Microspouters

Ali Shademani, Hongbin Zhang,\* John K. Jackson, and Mu Chiao\*

Triggerable devices capable of on-demand, controlled release of therapeutics are attractive options for the treatment of local diseases because of their potential to enhance therapeutic effectiveness with reduced systemic toxicity. Here, the design and fabrication of a miniaturized device, termed a microspouter, is described. This device is shown to provide active and precise control of localized delivery of drugs on demand. The microspouter is composed of a magnetic sponge to provide the force for drug release through magnetic field-induced reversible deformation, a reservoir for the sponge installation and drug loading, and a soft membrane for sealing the device. Following application of a magnetic field to the microspouter, the shrinking of the sponge may trigger a spouting of drug through a membrane's microaperture. The efficiency of the device in controlling the dose and time course of drug release under different external magnetic fields has been demonstrated using methylene blue and docetaxel as model drugs. Additionally, the microspouter is found to have low background drug leakage that allows for tunable drug release in an *ex vivo* implantation experiment. All the results confirm the microspouter as a potential device for safe, long-time, and controlled drug release in local disease treatment.

## 1. Introduction

The goal of drug delivery technology is to provide a safer, more efficient, and convenient means of drug administration to improve therapeutic effectiveness. Over the past few decades, numerous drug delivery systems ranging from nanoscale to macroscale devices have been developed to present different release patterns, such as sustained zero-order release,<sup>[1,2]</sup> environment-responsive release,<sup>[3,4]</sup> differential release,<sup>[5-7]</sup> targeted release,<sup>[8,9]</sup> and so on. Drug release from most of these systems is through a passive manner with a predetermined release rate, which basically cannot be modified after administration. However, this monotonic drug release with an untunable release

rate may not always be appropriate in disease treatment where the required release kinetics may be variable, such as in the treatment of diabetes,<sup>[10]</sup> where the required dosage and timing of insulin delivery may vary largely from patient to patient. Thus, systems capable of active and sustained regulation of drug presentation to precisely determine the location, timing, and dose magnitude, would be more beneficial for the delivery of drugs such as hormones, painkillers, and chemotherapeutic drugs.<sup>[11,12]</sup>

Macroscale triggerable systems that can release drug via the triggering of externally applied physical signals, such as ultrasound,<sup>[13,14]</sup> temperature,<sup>[15,16]</sup> electric,<sup>[17,18]</sup> magnetic fields,<sup>[19,20]</sup> and light,<sup>[21,22]</sup> are gaining attention in medicine. These triggerable drug delivery systems allow a spatiotemporal management of drug availability at a disease site controlled by the patient or physician using a remote device.<sup>[11,12,23]</sup> Moreover, they have

the advantages of being able to accommodate a large quantity of drug and achieve multiple dosing after a single administration through repeated triggering. Polymeric systems for triggerable drug delivery such as ferrogels,<sup>[24,25]</sup> polyelectrolyte hydrogels,<sup>[26,27]</sup> and light-sensitive matrices<sup>[28,29]</sup> have been studied. Drug release from these systems could be accelerated through mechanisms including ultrasound/light-mediated degradation or electromagnetic field-induced deformation of matrices.<sup>[11,30]</sup> Unfortunately, there are some disadvantages such as an initial burst of drug release or a relatively large drug leakage via diffusion, which are difficult to avoid because most of these systems are fully exposed to surrounding environments. Furthermore, with the possible degradation of the matrix and a decrease of payload, the stability and reliability of these systems may reduce rapidly over time and prevent reproducible drug dosing.

Implantable reservoir-based devices have also been designed to trigger controlled drug release. Some are electrochemically driven microdevices consisting of a drug-filled microreservoir sealed with a thin metallic electrode (commonly a gold membrane).<sup>[31-33]</sup> When an electrical potential is applied to the device, the top gold membrane is dissolved and the contained drug solution diffuses out. Nevertheless, once the reservoir is exposed, the release cannot be stopped and the drug amount discharged each time is predetermined, not flexible. Another type of device is a composite membrane made from

A. Shademani, Dr. H. Zhang, Prof. M. Chiao  
Department of Mechanical Engineering  
The University of British Columbia  
Vancouver, BC V6T 1Z4, Canada  
E-mail: izhanghongbin@gmail.com;  
muchiao@mech.ubc.ca

J. K. Jackson  
Department of Pharmaceutical Sciences  
The University of British Columbia  
Vancouver, BC V6T 1Z3, Canada



DOI: 10.1002/adfm.201604558

an ethylcellulose film with embedded thermosensitive poly(*n*-isopropyl acrylamide) (polyNIPAm)-based nanogels and magnetic nanoparticles, which was reported by Hoare et al.<sup>[34,35]</sup> These membranes could trigger the reversible shrinkage of the nanogels and increase the permeability of the membrane for drug release by heating the membrane with magnetic nanoparticles in the presence of an oscillating magnetic field. These oscillating magnetic field-heated membrane systems need a relatively long time (more than 30 min for one release duration) to trigger drug release and obtain a desired release amount, as the mechanism relies on passive diffusion along a concentration gradient. Cai et al. used Fe<sub>3</sub>O<sub>4</sub> particles inside the drug reservoir to block/open the pores of a membrane covering on the reservoir, achieving a reversible switching of drug flux.<sup>[36]</sup> However, one challenge associated with such a system might be that, during both on and off periods of the device, an oriented magnetic field is required to be applied and maintained from opposite directions, which may affect its convenience in application. Drug release triggered by the deformation of a membrane covering the drug reservoir under magnetic fields was also investigated.<sup>[37–39]</sup> However, due to limitations of the membrane deflection, the driving force for drug release was limited and a relatively longer magnetic stimulus was needed to avoid reabsorption of the drugs by the device.

Although various remotely activated drug delivery systems have been developed, there have been few reports of devices capable of repeated and quickly switching between “on” and “off” states to realize an accurate control of on-demand drug release. In this study, a magnetic-driving drug delivery device—a microspouter that consisted of a polydimethylsiloxane (PDMS) reservoir, a thin membrane, and a magnetic sponge, was designed and fabricated. Different from diffusion-based drug release mechanisms, the microspouter is driven by the sponge and can perform on-demand drug release instantaneously through a spouting triggered by external magnetic fields.

The stability and reproducibility of the microspouter for repeatable, quick, on-demand release were investigated by *in vitro* and *ex vivo* drug release experiments using methylene blue (MB) and docetaxel (DTX).

## 2. Results and Discussion

### 2.1. Magnetic Sponges: Preparation and Characterization

Stochastic porous structures made through different methods such as gas-foaming,<sup>[40]</sup> freeze-drying,<sup>[24,25]</sup> and 3D printing,<sup>[41]</sup> have been increasingly attractive for biomedical applications. In this study, porous magnetic sponges were created to provide a force for drug release using a sugar mold method (see the Experimental Section).<sup>[42,43]</sup> In this case, it requires that the sponges can deform quickly and reversibly in response to magnetic fields. To achieve this purpose, PDMS elastomers were fabricated with 3D connected macropores and incorporated with ferromagnetic carbonyl iron (CI) microparticles. PDMS was chosen as the matrix material for the sponge because of its chemical inertness, elasticity, ease of fabrication, and low manufacturing costs.<sup>[44–46]</sup>

To make the magnetic PDMS scaffolds, different amounts of CI microparticles were mixed well with the PDMS prepolymer liquid first, followed by pouring the mixture into a sugar mold and curing at 70 °C for 3 h (detailed description on the preparation is presented in the Experimental Section). The weight ratio of CI to PDMS may affect the magnetomechanical properties of the sponge. For example, increasing CI content may enhance the magnetic properties of the sponge but at the same time lead to a stiffer sponge with a higher Young’s modulus. As a proof of concept study, magnetic sponges (Figure 1a) with different concentrations of CI microparticles (50, 100, and 150 w/w%) were first developed, in which interconnected pores (Figure 1b)

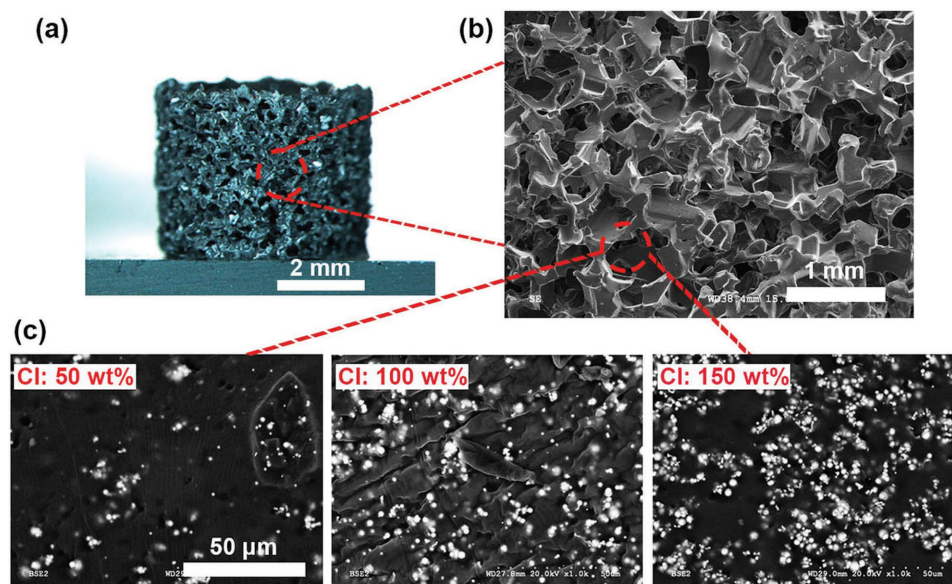


**Figure 1.** a) Photograph of a magnetic sponge cylinder. b) SEM image of the morphology of porous PDMS sponge. c) magnified SEM images of sponges with different CI to PDMS weight ratios (left: 50 w/w%; middle: 100 w/w%; right: 150 w/w%).

were formed using the same water-soluble sugar template. Although the porosity of the sponge might also affect the mechanical properties, the pore size of the PDMS sponge in this study was fixed to around 200–500  $\mu\text{m}$  and the porosity (the ratio of the vacant space volume to the sponge apparent volume) was  $0.64 \pm 0.02$ . The high proportion of pores might confer a high elasticity to the sponge and therefore generate a large deformation under an external force. The dispersion of CI microparticles in the sponge matrix was also observed (Figure 1c). The white dots were the embedded CI microparticles with a diameter about 4–7  $\mu\text{m}$ , which exhibited a relatively homogeneous distribution and became more evident when its concentration increased.

The deformation of these macroporous scaffolds under the influence of varying magnetic fields was next investigated. Figure 2a shows the configuration changes of a typical sponge cylinder (CI/PDMS = 100 w/w%) at different magnetic field strengths applied with a magnetic bar from the bottom of the sponge. Its height reduced more when it was subjected to stronger magnetic fields. The height variations were further compared on sponges of different CI concentrations (Figure 2b). Generally, increasing the CI particle concentration might generate a larger magnetic force exerted on the sponge in a given magnetic field and consequently increase the volume change. It can be seen that the sponge with the lowest CI concentration, CI/PDMS = 50 w/w%, gave the least deformation. However, the sponge with CI/PDMS = 150 w/w% presented less displacement in various magnetic fields in comparison with the 100% one. Following this discovery, the compressive moduli of these two sponges were measured (Figure 2c) through the stress–strain curves obtained from a compression test (see the Experiment Section), which gave values of 5.02 and 6.52 kPa for the sponges of 100 and 150 w/w%, respectively. The increased modulus was likely due to the enhanced rigidity of the sponge stemming from the excess addition of CI microparticles, which weakened the effect of magnetic field on the sponge deformation. Hence, the most magnetically sensitive sponge of CI/PDMS = 100 w/w% in the study was chosen for the microspouter fabrication.

## 2.2. Fabrication of the Microspouter

The PDMS reservoir was made using a 3D-printed positive mold (Figure 3a). After being demolded, a round shape reservoir (Figure 3b) with a depth of 1.5 mm and diameter of 4 mm

was punched out, where the magnetic sponge was subsequently installed and the drug was loaded. Then, a thin PDMS membrane was permanently bonded to the top of the reservoir and sponge through plasma treatment to seal the microspouter. (The sealing condition by the membrane was confirmed by a leakage test, see Supporting Information.) Finally, an aperture ( $90 \times 90 \mu\text{m}^2$ ) was made at the center of the membrane (Figure S1, Supporting Information) by laser ablation using a Nd:YAG laser (Quicklaze, New Wave Research, Sunnyvale, CA, USA). The detailed structure was also presented in the diagrammatic sketch (Figure 3c) and in the cross-section scanning electron microscope (SEM) image (Figure 3d), clearly showing the three major components of a microspouter. Moreover, no

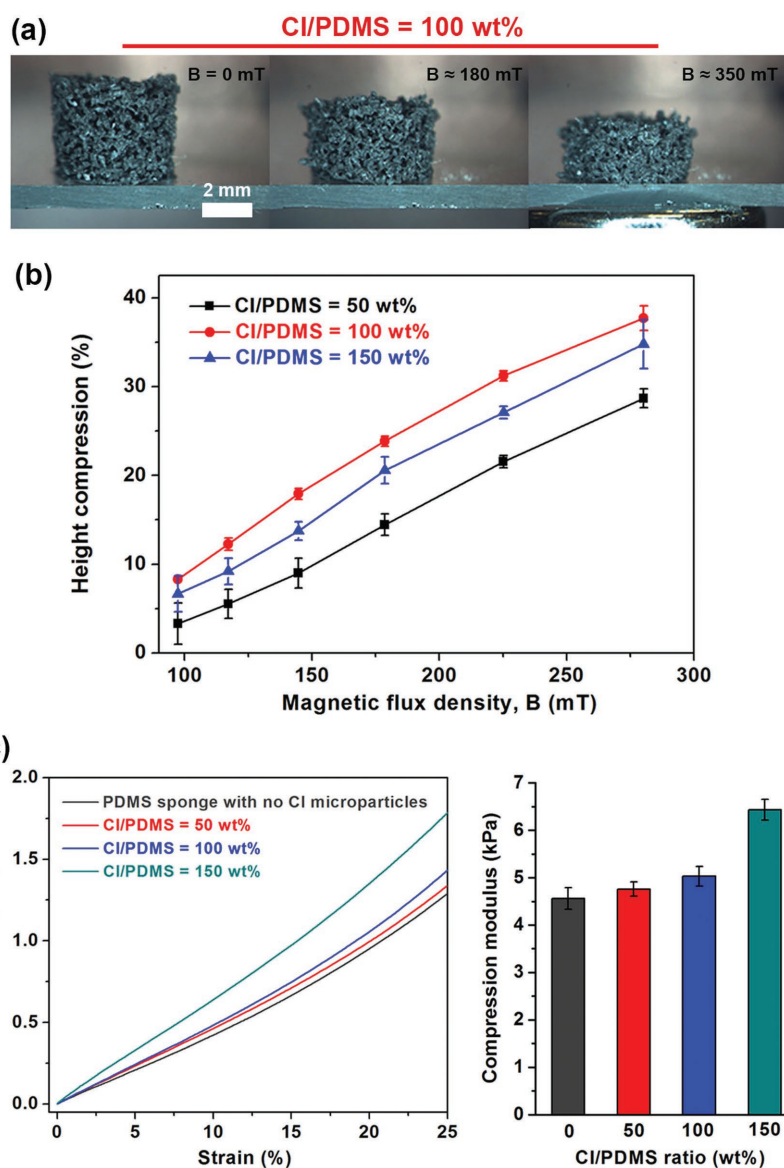


**Figure 2.** a) Images of sponges deformed under different magnetic field strengths. b) Height compression of magnetic sponges with different CI/PDMS w/w% ratios versus various magnetic fields. c) Stress versus strain curves from compression tests and compressive moduli for sponges with different CI/PDMS ratios. The error bars represent mean  $\pm$  standard deviation ( $n = 3$ ).

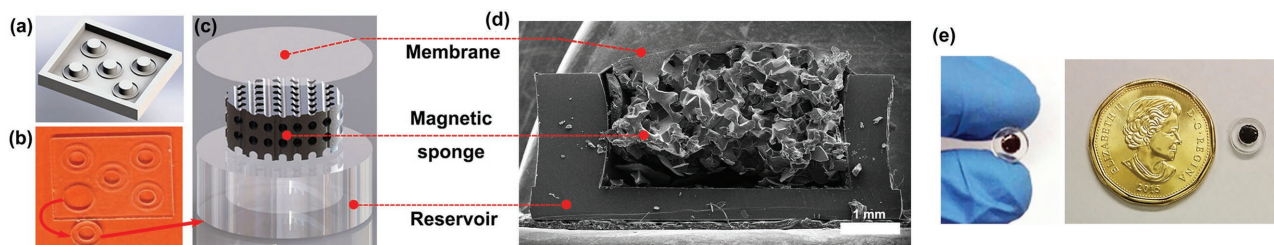


**Figure 3.** a) 3D-printed mold for reservoir fabrication. b) Image of demolded PDMS layer and one typical reservoir punched out. c) Schematic-exploded diagram of the device components. d) SEM image of the device from the cross-section view. e) Images of the microspouter.

separation was observed at the bonding areas between the membrane and the reservoir, and between the membrane and the sponge (Figure S2, Supporting Information), confirming that a firm and reliable sealing of the microspouter by the membrane was achieved. The final assembled microspouter was shown in Figure 3e. The black part was the magnetic sponge and the outer transparent part was the reservoir.

### 2.3. Release of Methylene Blue

We hypothesized that the sponge deformation induced by magnetic fields could haul the membrane down to the reservoir and increase the pressure in the microspouter, which would trigger drug release by spouting drug solution (Figure 4a). To test this hypothesis, MB was first chosen as a good water-soluble model drug. Before a release step was performed, drug-loaded microspouters were degassed and infused with distilled water in a vacuum chamber to dissolve drugs in the reservoir. Afterwards, the microspouter containing 200  $\mu\text{g}$  MB was placed in distilled water and the MB release was triggered every 10 min by actuating the microspouter in a 120 mT magnetic field for 5 s. As shown in Figure 4b and Movie S1 (Supporting Information), with a magnetic stimulation, the MB solution was released strongly and spouted like a fountain, while negligible drug diffusion through the aperture was observed without actuation. The cumulative release profile exhibited a steady stepwise increment with magnetic stimulations (Figure 4a). The released amount of MB in each actuation was about 2.34  $\mu\text{g}$  ( $n = 36$ ), which was around 37 times more than its leakage (about 0.064  $\mu\text{g}$ ) during two sequent actuations (Figure 4b). The background release of MB in a period of 24 h by diffusion from the device was about  $24.96 \pm 2.16 \mu\text{g}$  ( $n = 3$ ) in an experiment lasting three consecutive days. It seems that, without the interference from a magnetic actuation, the diffusion was relatively slower than was observed during the intervals of two actuated releases. On the other hand, compared to the device with no sponge inside, which had a background leakage rate about  $1.95 \pm 0.21 \mu\text{g h}^{-1}$  ( $n = 3$ ), the background leakage rate of the device with the sponge was about  $1.04 \pm 0.09 \mu\text{g h}^{-1}$  ( $n = 3$ ), half of the former. Thus, the relative low background release of MB with high water solubility probably resulted from the small size of the aperture ( $90 \mu\text{m} \times 90 \mu\text{m}$ ) and the presence of the porous sponge in the reservoir, which to some extent impedes drug diffusion and consequently the leakage in the dormant phase of the device. The MB release triggered by magnetic fields of different strengths was also measured. The release in each

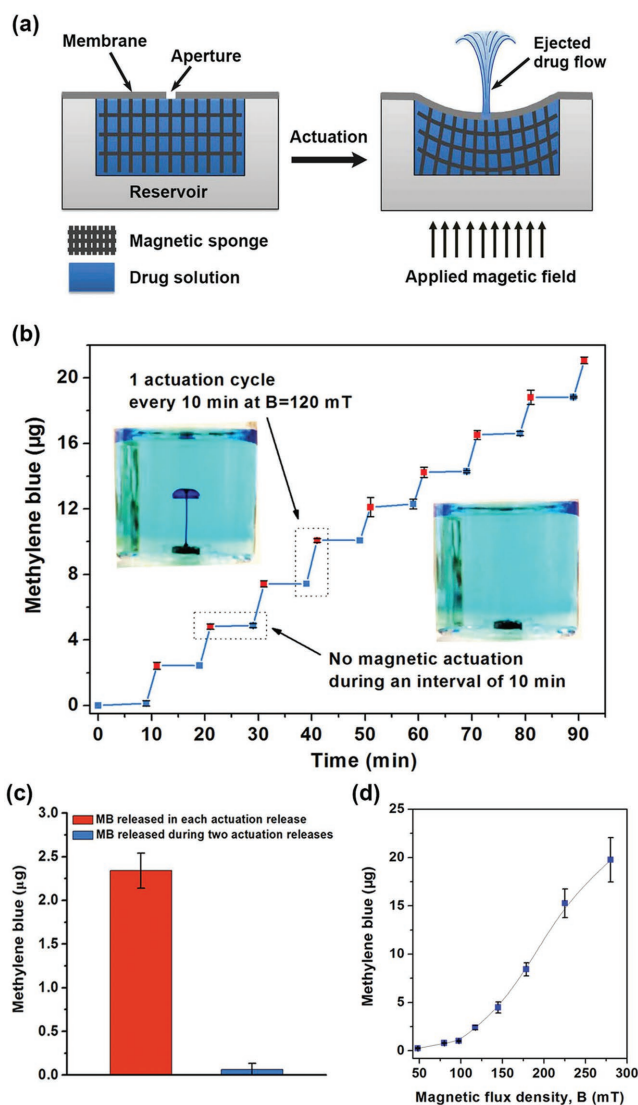


**Figure 4.** a) A schematic diagram showing the release mechanism of the microspouter. b) Cumulative methylene blue (MB) release profile by magnetic stimulations and images of MB release with and without magnetic stimuli. c) Released amounts of MB in an actuation ( $n = 36$ ) and during the dormant phase between two actuations. d) MB release in an actuation under different magnetic field strengths. The error bars represent mean  $\pm$  standard deviation ( $n = 3$ ).

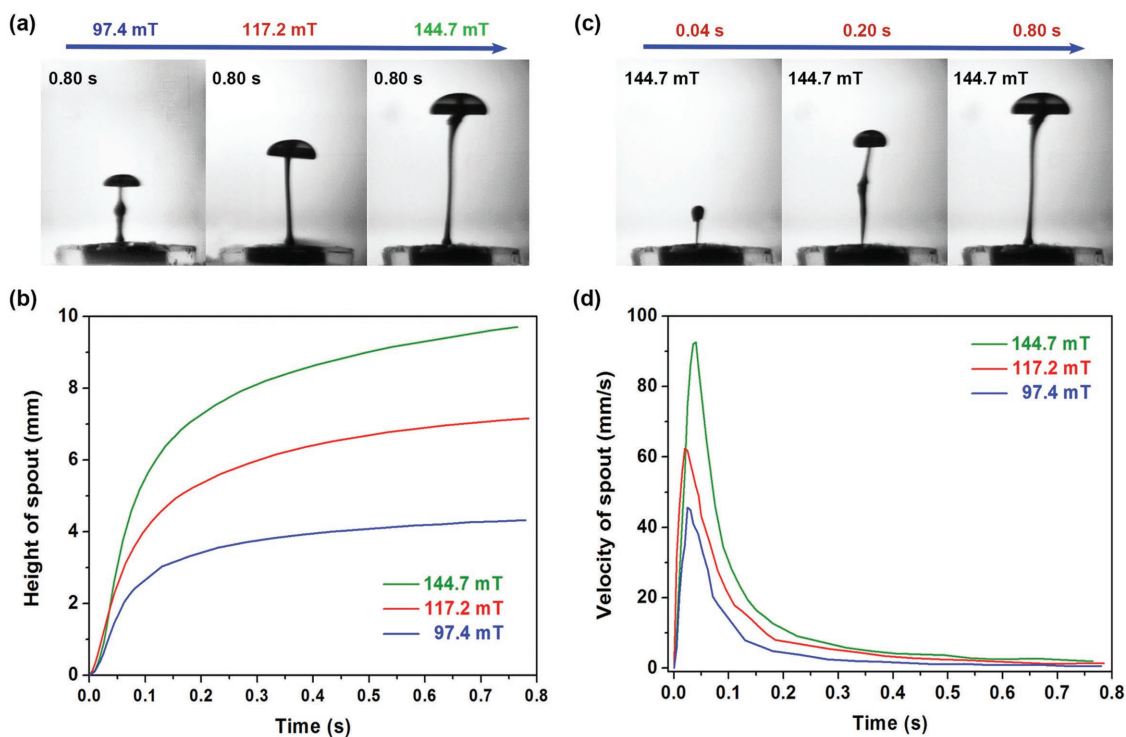


**Figure 5.** a) Camera images of flows spouted from the microspouter at 0.80 s under different magnetic field strengths. b) Tip positions of spouts versus time under different magnetic fields. c) The images of spouts formed at different time points under a magnetic field strength of 144.7 mT. d) Estimated velocities of the jet flows based on numerical analysis.

actuation increased from 0.24  $\mu\text{g}$  at 48 mT to 19.75  $\mu\text{g}$  at 280 mT because more drug solution was ejected by a larger sponge deformation at a stronger magnetic field. This suggested that the drug release from the microspouter could be easily tuned by applying different magnetic fields. However, the amount of drug release did not exhibit a linear increase with the strength of the magnetic field. Under magnetic fields of relatively low strength, drug release increased very slowly with the magnetic field strength. However, in the range of relatively high magnetic field strengths, the drug released much more with the increased strength. The result could be ascribed to a drug reabsorption phenomenon of the device. When the applied magnetic field was removed from the device, a part of the released drug surrounding the aperture may be reabsorbed back into the reservoir due to the relaxation of the sponge, which could be observed in Movie S1 (Supporting Information). The drug reabsorption may be influenced more significantly under low magnetic field strengths because most of the ejected drug would be closer to the aperture due to the low height of ejection. However, under a magnetic field of high strength, the drug solution could be effectively released to decrease the reabsorption by an ejection far away from the aperture. Thus, a quick increase of drug release was observed.

#### 2.4. Evaluation of the Jet Flow from the Microspouter

As seen during MB release (Figure 4a), the microspouter was able to spout the drug solution far into the medium in a

manner that was proportional to the applied magnetic field strength. To further evaluate the drug release behavior from the microspouter, the jet flows of MB under various magnetic fields and at different time points were observed using a phantom high speed camera (Figure 5a,c). The range of jet flows was computed based on the distance from jet flow's tip position to the aperture of the microspouter. The maximum travel distance was about 4.5, 7.5, and 10 mm triggered by a 97.4, 117.2, and 144.7 mT magnetic fields, respectively (Figure 5b), and the estimated tip velocity was 45, 62, and 92  $\text{mm s}^{-1}$  in the aforementioned magnetic field strengths, respectively (Figure 5d). The high velocity may ensure a quick and efficient drug release at a desired time point and promote drug diffusion to reach the target area. These results demonstrated that the drug dosage and its penetration depth can be directly controlled by the externally applied magnetic fields.

#### 2.5. Release of Docetaxel

In addition to the release of a hydrophilic drug (MB), a hydrophobic drug with poor water solubility, DTX (water solubility 5  $\mu\text{g mL}^{-1}$ ), was selected to assess the functionality of the microspouter for controlled drug release. DTX is a taxane-based drug used clinically to treat many types of cancer diseases by hindering and impeding cell replication, leading to the inactivation and death of tumor cells. DTX release was conducted by actuating the microspouter every 20 min for one actuation consisting of 5 on/off cycles. In every cycle, the microspouter

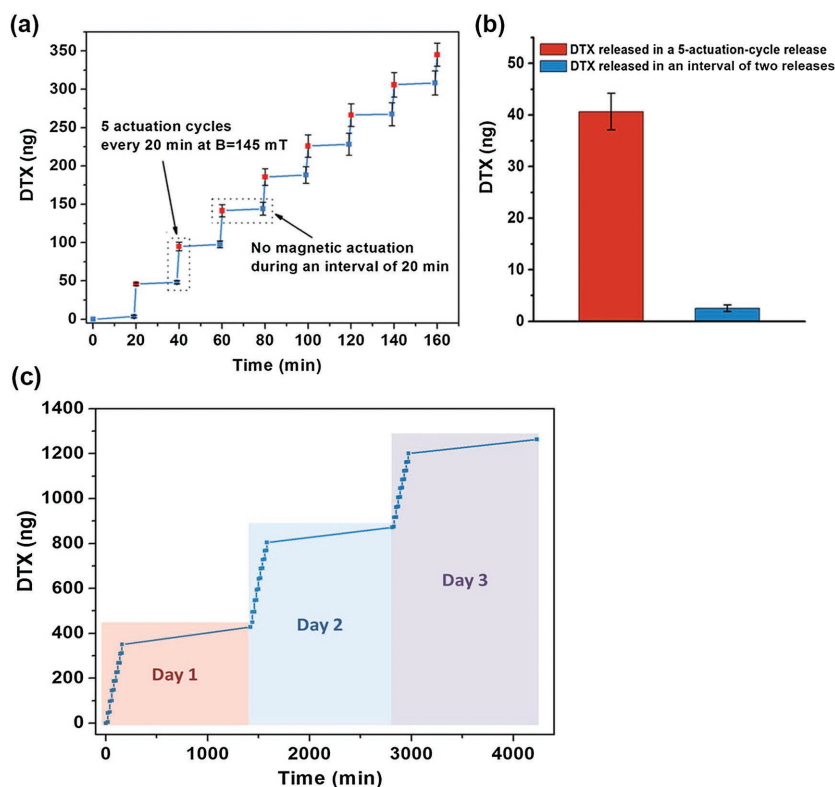


**Figure 6.** a) Cumulative docetaxel (DTX) release profile by magnetic stimulations. b) Released amounts of DTX in an actuation ( $n = 24$ ) and during the dormant phase between two actuations. c) 3 d consecutive DTX release; each day device was actuated for eight times, each time consisting of five actuation cycles. The error bars represent mean  $\pm$  standard deviation ( $n = 3$ ).

was exposed to the predefined magnetic field of 145 mT for 7 s (on), followed by 5 s of relaxation (off), which took about 1 min for each actuation. Similar to the release of MB, the cumulative release profile of DTX (Figure 6a) also presented a significant stepwise increase with application of the magnetic field. The released DTX was about 40.64 ng ( $n = 24$ ) in each actuation, and the leakage during two consecutive actuations was about 2.41 ng (Figure 6b). The release of drug at each actuation interval was very uniform, potentially allowing for very accurate and reproducible dosing.

To further demonstrate the repeatability of drug release by the microspouter, the same release pattern was repeated in three consecutive days. As seen in Figure 6c, the DTX release in Day 1 could be repeated in Day 2 and Day 3 with the same release conditions. The background leakage with no magnetic stimulation over 20 h during the releases between two following days was about 72 ng, which meant that only 0.06 ng DTX diffused out of the microspouter per minute. This negligible leakage proved that the microspouter had an effective encapsulation for drugs before being activated. Furthermore, it was noted that the cumulative release of DTX after 3 d was just 0.32% of the preloaded drug (400  $\mu$ g) in the microspouter, indicating that a DTX-loaded device might have a very long life expectancy before the drug payload was exhausted. The quite low exhaustion rate of DTX could be ascribed to its low water-solubility (that was increased from 5  $\mu$ g mL<sup>-1</sup> in water to 70  $\mu$ g mL<sup>-1</sup> by using bovine serum albumin (BSA)/phosphate buffered saline

(PBS) solution<sup>[39]</sup> in the experiment), which also partially contributed to the good reproducibility of the on-demand drug release. Since there was always an excess of drug in the reservoir (400  $\mu$ g) and the volume of the drug solution ejected each time is relatively small, the internal drug concentration in the reservoir would not reduce much and could quickly get resaturated (especially with the internal movement in the reservoir generated by the sponge deformation). This may result in the drug solution that was ejected during the actuation being approximately saturated, allowing for good control of drug release by the device.

## 2.6. Inhibition Assessment of PC3 Cell by Docetaxel

Drug effectiveness may be reduced due to degradation or metamorphism from improper encapsulation and storing, especially for some sensitive drugs.<sup>[47,48]</sup> This is especially true for water soluble drugs stored in solution (e.g., in vivo in a device that was flooded with water waiting for actuation). Using our method, drugs may be loaded in solution or solid states. The formed devices can be stored in a vacuum environment to protect drugs from oxidation. To assess the efficacy of DTX released from the

microspouter, its influence on cell viability of prostate cancer PC3 cells was investigated and compared with fresh DTX. As illustrated in Figure 7, cell viability decreased with increasing DTX concentration. Both fresh DTX and DTX released from the device exhibited almost the same inhibition to cell proliferation (the cell proliferation drastically decreased to 40%

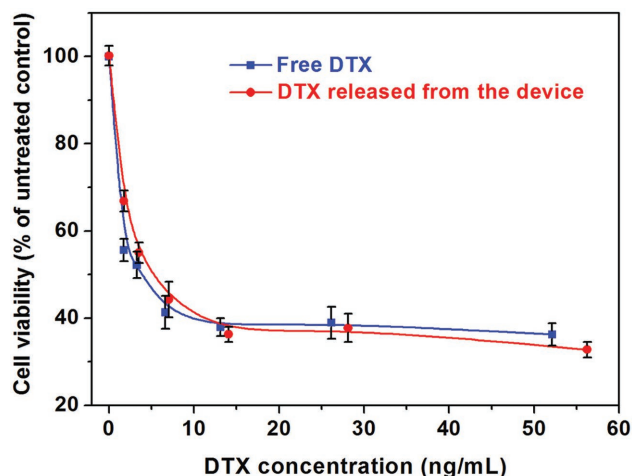


**Figure 7.** Inhibition of PC3 cell proliferation using the DTX released from actuation experiments in comparison with fresh DTX. The error bars represent mean  $\pm$  standard deviation ( $n = 3$ ).

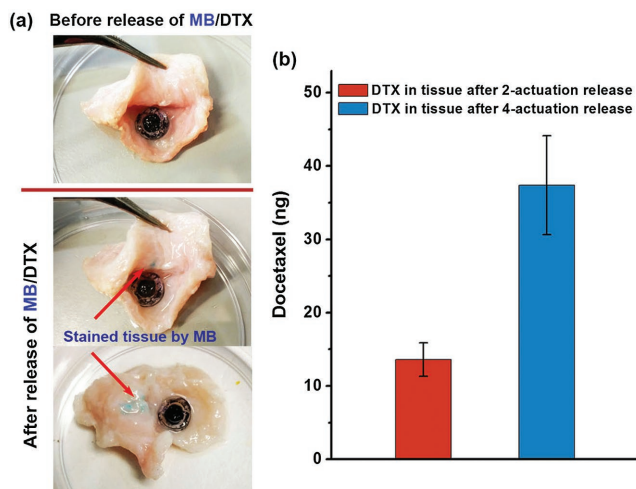


**Figure 8.** a) Drug (MB/DTX) release from implanted microspouter inside a piece of porcine bladder tissue, the MB stained area labeled the target area of drug release. b) DTX intakes at the targeted site of tissues after two and four times actuation. The error bars represent mean  $\pm$  standard deviation ( $n = 3$ ).

when the concentration of DTX was about  $10 \text{ ng mL}^{-1}$ ). The close cell inhibition behaviors of released DTX and fresh DTX demonstrated that the drug stored inside the device can keep its effectivity and activity even after more than one month of encapsulation.

## 2.7. Ex Vivo Tissue Implantation and DTX Uptake

Finally, the capability of microspouters for controlled localized drug delivery was examined in an ex vivo tissue implantation model (pig's bladder pocket). The DXT/MB-loaded microspouter was placed inside a piece of porcine bladder tissue and the drug release was triggered by a 280 mT magnetic field. After magnetic actuations, the target sections that were stained to blue by MB (Figure 8a) were cut out and digested to measure the DTX uptake by tissue. The total DTX released to the target tissue in this protocol was about  $13.6 \pm 2.3 \text{ ng}$  when the tissue was subjected to two actuation cycles (Figure 8b). The mass of each tissue sample was also measured, which resulted in a DTX concentration of  $33.21 \pm 5.49 \text{ ng cm}^{-3}$ , as the measured tissue density was about  $1 \text{ g cm}^{-3}$ . These DTX concentrations in tissue were in the effective range of DTX in cancerous tissues according to the PC3 cell study, where concentrations around  $10 \text{ ng mL}^{-1}$  ( $10 \text{ ng g}^{-1}$  equivalent) were effective at inhibiting cancer cell proliferation (Figure 7). In another protocol, this device was subjected to four actuation cycles which caused the released DTX to increase to  $37.39 \pm 8.75 \text{ ng}$ . Therefore, this device demonstrated local drug release after implantation with evidence of adjustable drug dosage in the tissue which was a function of the number of actuations. As the working environment is more complex in body than in vitro and possible biofouling issues may arise, long term in vivo performance of the microspouter will be further investigated and presented in our future work.

## 3. Conclusion

We proposed a new drug delivery device, a microspouter assembled from a magnetic sponge, a reservoir, and a soft membrane, to offer a precisely controllable way for on-demand local drug delivery. The microspouter provides a tunable force to trigger drug release by reversible magnetic sponge deformation using extrinsic magnetic stimulations and a relatively large reservoir for a large quantity of drug encapsulation. The large geometric deformation and high levels of spouting arising from the sponge shrinkage may provide a robust release mechanism that offsets tissue compaction or aperture blockage problems that might possibly occur with less forceful release systems. When using this implantable microspouter, drug presentation including releasing time and dose can be easily and reliably controlled by patients to fit the prescribed needs. Moreover, the microspouter has the potential to achieve a safe and long term drug release due to a very low background leakage and large drug loading ability. All these features make the microspouter an ideal device for controllable, on-demand drug administration in local treatment of diseases.

## 4. Experimental Section

**Preparation of Characterization Magnetic Sponges:** 20 g granulated household sugar was thoroughly mixed with 0.5 mL water to get the sugar wetted and pressed firmly in a Petri dish (5 cm in diameter). The Petri dish was subsequently placed in a convection oven to dry the material to form a mold of connected sugar particles. PDMS prepolymer and curing agents (Sylgard 182, Dow Corning) were mixed by a weight ratio of 30:1, followed by the addition of CI microparticles (4–7  $\mu\text{m}$  in diameter, Chemical Store Inc., USA) at weight ratios of 50%, 100%, and 150% (CI/PDMS w/w%). The well-mixed PDMS/CI was then poured onto the prepared sugar mold. After penetration of the liquid through the sugar mold in a vacuum chamber, the PDMS mixture was cured in an oven at  $70 \text{ }^\circ\text{C}$  for 3 h. The cured magnetic PDMS was cut into cylinders, which were then immersed in water to dissolve the sugar and form porous magnetic PDMS sponges.

**SEM Observation:** Tescan Mira3 XMU field emission SEM was employed to observe the inner morphologies of magnetic sponges. The samples were first coated with gold by vacuum sputtering before observation under SEM.

**Porosity Measurement:** Dried sponge cylinders ( $\approx 5 \times 6.5 \text{ mm}$ , diameter  $\times$  height) were weighted and placed in distilled water. The sponges were first gently compressed using a magnet and then degassed under vacuum for 20 min to let water fully fill in pores. After that, the sponges full of water were taken out and weighted again to calculate the volumes of water in the sponges ( $V_w$ ). The porosity of the sponge was finally determined by the volume of sponge cylinder ( $V_s$ ) and the volume of water it contained as  $V_w/V_s \times 100\%$ . Three separate samples from independently fabricated molds were used in the experiment to get the average porosity of the sponge.

**Measurement of Sponge Deformation under Magnetic Fields:** Magnetic sponge cylinders with different contents of CI were placed on a glass slide. A magnetic field was applied from different distances between the sponge and a magnetic bar. The deformation of sponge cylinders under different magnetic field strength was recorded and presented as the displacement of the top surface. Three separate samples from independently fabricated molds were used in the deformation measurement.

**Compression Test:** The elasticity modulus of all samples with different ratios (50%, 100%, 150%) including a porous PDMS (without CI particles) were measured using thermomechanical analyzer (TMA

2940-Q series, TA, Instruments, DE, USA). Samples used were 5 mm in diameter and 6 mm in height) and compressed with a ramp force of 0.015 N min<sup>-1</sup> to achieve 25% strain.

**Preparation of PDMS Reservoirs and Membranes for the Microspouters:** The reservoirs of microspouters were fabricated using a positive mold that was designed with Solidworks software and built using a 3D printer (Asigo Pico). The positive mold consisted of pillars with the height of 1.5 mm and the diameter of 4 mm. For the reservoir fabrication, a PDMS (Sylgard 184, Dow Corning) mixture was made at a cross-linker to base ratio of 1:10, and poured into the mold. After being degassed in a vacuum chamber for 30 min, the mold with liquid PDMS was placed in an oven to cure PDMS at 70 °C for 3 h. The cured PDMS was demolded (peeled off from the mold) to get the reservoir. The final thickness of the reservoir was less than 2 mm.

A PDMS membrane with a thickness of about 10 μm for sealing the microspouter was manufactured next. First, a polyacrylic acid (PAA) solution was prepared by dissolving PAA powder ( $M_w = 1800$ , Sigma-Aldrich) in distilled water at a 25% w/v concentration and filtered using a sterile 0.45 μm PVDF syringe filter (Millipore Corporation, USA). Second, a glass slide was treated by plasma for 30 s in roughly 700 mTorr pressure and then coated with PAA using a spinner with 500 rpm for 10 s and then 800 rpm for 30 s. The glass slide was then placed on a hot plate of 150 °C for 5 min to dry the PAA coating which was used as a sacrificial layer for PDMS membrane. Finally, liquid PDMS was spun on the glass slide (20 s at 500 rpm, 3 min at 3500 rpm) and cured on the hot plate at 150 °C for 5 min to form the PDMS membrane.

The final device was prepared by assembling the aforementioned components. Initially, the drug was loaded at the desired amount in the reservoir. The magnetic sponge was later placed into the reservoir and the device was further sealed with the membrane by applying plasma surface treatment on the top surface of reservoir, sponge, and the membrane. By dissolving the sacrificial layer (PAA) in water, the device was set free and an aperture (90 × 90 μm<sup>2</sup>) was eventually created at the center of the membrane using laser ablation.

**Release of MB and DTX:** MB (Sigma-Aldrich) and DTX (Sigma-Aldrich) were used as model drugs to test the drug release performance of the microspouter. The loading amounts of drugs in a microspouter were 200 μg for MB and 400 μg for DTX. Before the MB release test, the microspouter was immersed in distilled water and placed in a vacuum chamber for 10 min to fill the microspouter's reservoir with water. For the DTX release test, the same process was carried out to fill the reservoir using PBS (pH 7.4), including 1% w/v BSA, instead of water.

For MB, the release experiment was performed using 5 mL of distilled water and every 10 min, the microspouter was actuated under a magnetic field of about 120 mTorr for 5 s. Before and after each actuation, 1 mL of medium was collected to measure the released MB. After that, equivalent fresh distilled water was complemented for following release. The MB concentration was determined using UV-vis spectrophotometer (50 BIO, Varian Medical Systems Inc., Palo Alto, CA, USA) at a wavelength of 662 nm.

For DTX, the release was performed in 5 mL PBS including 1% w/v BSA. Every 20 min, the microspouter was actuated under a magnetic field of about 145 mT for 7 s (on), followed by 5 s of relaxation (off). Five on/off cycles were included in each actuation which took about 1 min for the whole process. To precisely measure DTX concentrations, tritium labeled DTX (50 μCi/200 μL) in ethanol (Moravek Biochemicals Inc., Brea, CA, USA) was mixed with 4 mg unlabeled DTX in dichloromethane which resulted in a DTX solution of 40 mg mL<sup>-1</sup> for drug loading. Finally, each microspouter contained 400 μg DTX. Before and after each actuation interval, two and three samples were taken out of medium (each sample was 500 μL), respectively. Subsequently, each sample was pipetted into scintillation vials containing 5 mL of Cytoscint liquid scintillation fluid (Fisher Scientific, Fair Lawn, NJ, USA). The scintillation vials were then stirred using a vortex mixer and the 3H-DTX was quantitated using a liquid scintillation counter (Tri-Carb, PerkinElmer, Waltham, MA, USA). Thereafter, the DTX contents were determined by the corresponding standard curves.

**Jet Flow Measurement from the Microspouter:** The jet flows of the microspouter under various magnetic fields were observed and recorded using a phantom high speed camera (Phantom Miro, V611, AMETEK Inc.). The position of tip of jet flows was computed by image processing based on its distance from the device aperture per time. The tip velocity was also estimated in different cases by numerical analysis of tip's position versus time using Matlab software.

**PC3 Cell Proliferation in Vitro with DTX:** PC3 cells were cultured in Dulbecco's modified eagle medium containing 10% fetal bovine serum and plated at 1500 cells per well in a 96-well plate. The plate with cells was next incubated overnight at 37 °C to achieve ≈15% confluence. 200 μL DTX in PBS solution with 1% w/v BSA, which released from the microspouter, was added to each well with varying concentrations from 2 to 52 ng mL<sup>-1</sup> (based on liquid scintillation determinations of drug concentration). Cells were further incubated for 3 d at 37 °C. Cell viability was determined using nonradioactive cell proliferation assay (MTS assay, Promega Corporation, Madison, WI, USA) using absorbance at 490 nm. The media and the drug were removed from the cells and 120 μL of fresh MTS solution was added to the cells and incubated for 2 h to allow for cell driven conversion of tetrazolium to formazan to occur.

**Ex Vivo Implantation of Microspouters and Drug Uptake by Tissue:** A microspouter containing 400 μg DTX and 50 μg MB as a visual aid was installed in a pocket of porcine bladder tissue (the pocket was dissected out using a scalpel). To protect the membrane from direct contact with tissue, a 1 mm-thick PDMS housing was situated on top of the microspouter wall. Inside, the tissue pocket was filled with 400 μL of 1% BSA (w/v) PBS solution. The tissue was then exposed to a 280 mT magnetic field to study drug release from the microspouter after implantation. After actuations, the microspouter was removed and the target section of the tissue, which was determined by MB staining, was cut and digested in an aqueous-based tissue solubilizer (Solvable, PerkinElmer, Inc., Waltham, MA, USA) for about 1 d. Afterwards, ≈3 mL Cytoscint liquid scintillation fluid was added and the amount of DTX in the tissue was determined by quantitating the radioactivity of the solution.

## Supporting Information

Supporting Information is available from the Wiley Online Library or from the author.

## Acknowledgements

This work was supported by an NSERC/CIHR CHRP Grant (CHRP 414087-12), NSERC Discovery Grant, Canada Foundation for Innovations and UBC's Institute for Computing, Information and Cognitive Systems (ICICS).

Received: September 2, 2016

Revised: November 8, 2016

Published online: December 27, 2016

- [1] Q. Wang, J. Wang, Q. Lu, M. S. Detamore, C. Berkland, *Biomaterials* **2010**, *31*, 4980.
- [2] H. Zhang, R. Hao, X. Ren, L. Yu, H. Yang, H. Yu, *RSC Adv.* **2013**, *3*, 22927.
- [3] E. Fleige, M. A. Quadir, R. Haag, *Adv. Drug Delivery Rev.* **2012**, *64*, 866.
- [4] C. Alvarez-Lorenzo, A. Concheiro, *Chem. Commun.* **2014**, *50*, 7743.
- [5] H. Zhang, C. Zhao, H. Cao, G. Wang, L. Song, G. Niu, H. Yang, J. Ma, S. Zhu, *Biomaterials* **2010**, *31*, 5445.

- [6] H. Zhang, G. Wang, H. Yang, *Expert Opin. Drug Delivery* **2011**, *8*, 171.
- [7] H. Zhang, Y. Dong, L. Wang, G. Wang, J. Wu, Y. Zheng, H. Yang, S. Zhu, *J. Mater. Chem.* **2011**, *21*, 13530.
- [8] X. Ma, N. Gong, L. Zhong, J. Sun, X.-J. Liang, *Biomaterials* **2016**, *97*, 10.
- [9] K. Ulbrich, K. Holá, V. Šubr, A. Bakandritsos, J. Tuček, R. Zbořil, *Chem. Rev.* **2016**, *116*, 5338.
- [10] American Diabetes Association, Insulin Administration, *Diabetes Care* **2004**, *27*, S106.
- [11] Y. Brudno, D. J. Mooney, *J. Controlled Release* **2015**, *219*, 8.
- [12] B. P. Timko, T. Dvir, D. S. Kohane, *Adv. Mater.* **2010**, *22*, 4925.
- [13] H. Jiang, K. Tovar-Carrillo, T. Kobayashi, *Ultrason. Sonochem.* **2016**, *32*, 398.
- [14] N. Huebsch, C. J. Kearney, X. Zhao, J. Kim, C. A. Cezar, Z. Suo, D. J. Mooney, *Proc. Natl. Acad. Sci. USA* **2014**, *111*, 9762.
- [15] K. S. Oh, S. K. Han, Y. W. Choi, J. H. Lee, J. Y. Lee, S. H. Yuk, *Biomaterials* **2004**, *25*, 2393.
- [16] J. Sjollem, R. J. B. Dijkstra, C. Abeln, H. C. van der Mei, D. van Asseldonk, H. J. Busscher, *J. Controlled Release* **2014**, *188*, 61.
- [17] K. C. Wood, N. S. Zacharia, D. J. Schmidt, S. N. Wrightman, B. J. Andaya, P. T. Hammond, *Proc. Natl. Acad. Sci. USA* **2008**, *105*, 2280.
- [18] X. Shi, Y. Zheng, C. Wang, L. Yue, K. Qiao, G. Wang, L. Wang, H. Quan, *RSC Adv.* **2015**, *5*, 41820.
- [19] N. S. Satarkar, J. Z. Hilt, *J. Controlled Release* **2008**, *130*, 246.
- [20] T. Y. Liu, S. H. Hu, T. Y. Liu, D. M. Liu, S. Y. Chen, *Langmuir* **2006**, *22*, 5974.
- [21] C. P. McCoy, C. Rooney, C. R. Edwards, D. S. Jones, S. P. Gorman, *J. Am. Chem. Soc.* **2007**, *129*, 9572.
- [22] B. Yan, J. C. Boyer, D. Habault, N. R. Branda, Y. Zhao, *J. Am. Chem. Soc.* **2012**, *134*, 16558.
- [23] B. P. Timko, D. S. Kohane, *Isr. J. Chem.* **2013**, *53*, 728.
- [24] X. Zhao, J. Kim, C. A. Cezar, N. Huebsch, K. Lee, K. Bouhadir, D. J. Mooney, *Proc. Natl. Acad. Sci. USA* **2011**, *108*, 67.
- [25] C. A. Cezar, S. M. Kennedy, M. Mehta, J. C. Weaver, L. Gu, H. Vandenberg, D. J. Mooney, *Adv. Healthcare Mater.* **2014**, *3*, 1869.
- [26] S. Murdan, *J. Controlled Release* **2003**, *92*, 1.
- [27] S. Kennedy, S. Bencherif, D. Norton, L. Weinstock, M. Mehta, D. Mooney, *Adv. Healthcare Mater.* **2014**, *3*, 500.
- [28] C. Alvarez-Lorenzo, L. Bromberg, A. Concheiro, *Photochem. Photobiol.* **2009**, *85*, 848.
- [29] C. de Gracia Lux, J. Lux, G. Collet, S. He, M. Chan, J. Olejniczak, A. Foucault-Collet, A. Almutairi, *Biomacromolecules* **2015**, *16*, 3286.
- [30] N. Kamaly, B. Yameen, J. Wu, O. C. Farokhzad, *Chem. Rev.* **2016**, *116*, 2602.
- [31] J. T. Santini, M. J. Cima, R. Langer, *Nature* **1999**, *397*, 335.
- [32] Y. Li, R. S. Shawgo, B. Tyler, P. T. Henderson, J. S. Vogel, A. Rosenberg, P. B. Storm, R. Langer, H. Brem, M. J. Cima, *J. Controlled Release* **2004**, *100*, 211.
- [33] A. J. Chung, Y. S. Huh, D. Erickson, *Biomed. Microdev.* **2009**, *11*, 861.
- [34] T. Hoare, J. Santamaria, G. F. Goya, S. Irusta, D. Lin, S. Lau, R. Padera, R. Langer, D. S. Kohane, *Nano Lett.* **2009**, *9*, 3651.
- [35] T. Hoare, B. P. Timko, J. Santamaria, G. F. Goya, S. Irusta, S. Lau, C. F. Stefanescu, D. Lin, R. Langer, D. S. Kohane, *Nano Lett.* **2011**, *11*, 1395.
- [36] K. Cai, Z. Luo, Y. Hu, X. Chen, Y. Liao, L. Yang, L. Deng, *Adv. Mater.* **2009**, *21*, 4045.
- [37] F. N. Pirmoradi, J. K. Jackson, H. M. Burt, M. Chiao, *Lab Chip* **2011**, *11*, 3072.
- [38] F. N. Pirmoradi, J. K. Jackson, H. M. Burt, M. Chiao, *Lab Chip* **2011**, *11*, 2744.
- [39] P. Zachkani, J. K. Jackson, F. N. Pirmoradi, M. Chiao, *RSC Adv.* **2015**, *5*, 98087.
- [40] C. Ji, N. Annabi, M. Hosseinkhani, S. Sivaloganathan, F. Dehghani, *Acta Biomater.* **2012**, *8*, 570.
- [41] N. Yang, L. Gao, K. Zhou, *Mater. Sci. Eng., C* **2015**, *56*, 444.
- [42] S. J. Choi, T. H. Kwon, H. Im, D. I. Moon, D. J. Baek, M. L. Seol, J. P. Duarte, Y. K. Choi, *ACS Appl. Mater. Interfaces* **2011**, *3*, 4552.
- [43] P. Si, J. Wang, J. Guo, S. Li, W. Cai, H. Xu, *New J. Chem.* **2015**, *39*, 6823.
- [44] H. Zhang, M. Chiao, *J. Med. Biol. Eng.* **2015**, *35*, 143.
- [45] H. Zhang, J. K. Jackson, C. Bian, H. M. Burt, M. Chiao, *Adv. Mater. Interfaces* **2015**, *2*, 1500154.
- [46] E. Lee, H. Zhang, J. K. Jackson, C. J. Lim, M. Chiao, *RSC Adv.* **2016**, *6*, 79900.
- [47] H. H. Tønnesen, *Int. J. Pharm.* **2001**, *225*, 1.
- [48] M. W. Tibbitt, J. E. Dahlman, R. Langer, *J. Am. Chem. Soc.* **2016**, *138*, 704.